EUROFUSION WP15ER-PR(15) 13390

E Nilsson et al.

Kinetic modelling of runaway electron avalanches in tokamak plasmas

Preprint of Paper to be submitted for publication in
Plasma Physics and Controlled Fusion

This work has been carried out within the framework of the EUROfusion Consortium and has received funding from the Euratom research and training programme 2014-2018 under grant agreement No 633053. The views and opinions expressed herein do not necessarily reflect those of the European Commission.

Kinetic modelling of runaway electron avalanches in tokamak plasmas

E. Nilsson[1], J. Decker[1], Y. Peysson[1], R.S Granetz[2],

F. Saint-Laurent[1], M. Vlainić[3,4]

10th February 2015

[1]CEA, IRFM, F-13108, Saint-Paul-lez-Durance, France

[2]MIT Plasma Science and Fusion Center, Cambridge, Massachusetts 02139, USA

[3]Department of Applied Physics, Ghent University, B-9000, Ghent, Belgium

[4]Institute of Plasma Physics AS CR, 18200 Prague, Czech Republic

Abstract

Runaway electrons can be generated in tokamak plasmas if the accelerating force from the toroidal electric field exceeds the collisional drag force owing to Coulomb collisions with the background plasma. In ITER, disruptions are expected to generate runaway electrons mainly through knock-on collisions [1], where enough momentum can be transferred via relativistic to slow electrons to transport the latter beyond a critical momentum, setting off an avalanche of runaway electrons. This paper shows that the avalanche effect is important even in non-disruptive scenarios.

The formation of runaway electrons generated from the combined effect of Dreicer and avalanche is studied with the LUKE code, a solver of the 3-D linearized bounce-averaged relativistic electron Fokker-Planck equation [2], through the calculation of the response of the electron distribution function to a constant parallel electric field. The model, which has been successfully benchmarked against the standard Dreicer runaway theory now describes the runaway generation by knock-on collisions as proposed by Rosenbluth [3]. Since such knock-on electrons are principally scattered off with a perpendicular component of the momentum with respect to the

local magnetic field direction, these particles are highly magnetized. Consequently, the momentum dynamics require a full 2-D kinetic description, since they are highly sensitive to the magnetic non-uniformity of a toroidal configuration. For this purpose, a bounce-averaged knock-on source term is implemented. Runaway formation through knock-on collisions is found to reduce strongly when taking place off the magnetic axis, since trapped electrons can not contribute to the runaway electron population.

Finally, the relative importance of the avalanche mechanism is investigated as a function of key parameters for runaway electron formation; the plasma temperature and the electric field strength. In agreement with theoretical predictions, the LUKE simulations show that in low temperature and electric field the knock-on collisions rapidly becomes the dominant source of runaway electrons and can play a significant role for runaway electron generation in non-disruptive tokamak scenarios.

1 Introduction

Runaway electrons have been observed in magnetic confinement fusion experiments during the operation of tokamaks [4]. They are also encountered in nature in solar flares and electric discharges associated with thunderstorms [5]. The dynamics of electrons in a plasma is governed by the balance between acceleration in an electric field and collisions with the plasma particles. Collisional friction forces acting on the electrons reach a global maximum at the thermal velocity (v_{th}) and decrease for higher velocities. In the presence of a strong toroidal electric field (E) collisional drag may consequently be too weak to counteract the acceleration of electrons, which may result in continuously accelerated electrons, known as runaway electrons. If the electric field exceeds the critical field [6]

$$E_c = \frac{n_e e^3 \ln \Lambda}{4\pi\varepsilon_0^2 mc^2}, \tag{1}$$

where n_e is the electron density and $\ln \Lambda$ the Coloumb logarithm, runaway electrons may be generated if no other loss mechanisms than the collisional drag are present [7]. The acceleration of electrons in a DC field that are initially above the critical momentum (p_c), defined as the minimum momentum for which collisions are too weak to prevent acceleration of the electrons by the electric field to even higher energies, is referred to as the Dreicer mechanism [6]. In addition, these relativistic electrons can undergo close collisions with bulk electrons and transfer part of their momentum so that also the target electrons may get kicked into the runaway momentum region, while the momentum of the primary electrons remains above the critical momentum. These knock-on collisions can therefore lead to multiplication of the number of runaway electrons, commonly referred to as runaway avalanche [3].

Methods to mitigate the formation of runaway electrons in tokamak plasmas are based on either increasing the plasma density and thereby E_c by so called

massive gas injection (MGI) [8] or by deconfining the runaway electrons before they can reach too high energy by the means of resonant magnetic perturbations (RMP) [9]. Even though such mitigation methods have been demonstrated in present tokamak experiments, they might not provide a solution for large tokamaks like ITER [10]. Therefore the formation of the runaway electron population is a topic in urgent need of investigation.

Intense beams of highly energetic runaway electrons can form in tokamaks during plasma disruptions, fast unstable events that lead to a sudden loss of plasma confinement. If runaway electrons strike the first wall of the tokamak vacuum vessel the local energy deposition can cause significant damage [1]. Regardless of the mechanisms that lead to the onset of a major disruption, the post-disruption phases usually have similar time evolution [11]. They start with a fast cooling of the plasma typically associated with ergodisation of the magnetic flux surfaces [12], referred to as the thermal quench, which occurs on a time scale on the order of a millisecond. Consequently the plasma resistivity ρ, that scales with the temperature as $T^{-3/2}$, increases rapidly. The toroidal electric field is proportional to the resistivity and increases dramatically in order to maintain the local current density. Since the resistive current diffusion is enhanced by the reduction of the plasma conductivity, the plasma current decays progressively, but on a much longer time scale. In this process, a fraction of the pre-disruptive plasma current is carried by runaway electrons.

Disruptions are interesting but complex processes for studying the birth of runaway electrons, since they include magnetohydrodynamic (MHD) instabilities, anomalous transport and complex evolution of the magnetic field topology [13]. However, the generation of runaway electrons does not necessarily require the extreme conditions found in disruptions. In low density plasmas, the electric field can exceed the critical electric field also during the current flattop in a quiescent plasma, free of equilibrium transients, or during current ramp up or ramp down. An advantage of studying runaway formation in these so called non-disruptive scenarios is that the key parameters for the runaway electron mechanisms, mainly the electric field strength, electron density and temperature, can be better diagnosed than in disruptions. Runaway electrons have been detected in non-disruptive scenarios in several of the existing tokamaks [14]. Quiescent plasmas with nested magnetic flux surfaces is therefore more suitable for studying the formation of runaway electrons. In this work the formation of runaway electrons generated from the combined effect of Dreicer and avalanche is studied with the LUKE code, a solver of the 3-D (one spatial and two velocity dimensions) linearized bounce-averaged relativistic electron Fokker-Planck equation [2]. The LUKE code handles arbitrary shapes of the flux surfaces, but in this work the magnetic flux surfaces are assumed to remain circular and concentric like in the Tore Supra tokamak. They are assumed to remain intact throughout the runaway formation process, an assumption that is too restrictive for the thermal quench in disruptive scenarios.

Estimates of the time scale of the thermal quench, defined as the time scale of the convective loss of the plasma along the field, is given in Ref. [13]

$$\tau_{TQ} = kaL^{2/3}B^{2/3}T_e^{-5/6} \ \ [\mathsf{ms}], \tag{2}$$

where $L = \pi qR$, B is the magnetic field strength, a is the minor radius, q is the safety factor, $k \approx 6$, R the major radius and T_e the temperature prior to the thermal quench near the plasma edge. Equation 2 predicts the time scale of the outflow of plasma from the core. The typical thermal quench time scale for a prescribed temperature evolution (Fig. 1a) and Tore Supra like parameters is compared with the collisional time scale

$$\tau(v) = \frac{4\pi\epsilon_0^2 m_e^2 v^3}{q_e^4 n_e \ln\Lambda}, \tag{3}$$

where the velocity $v = v_{th}$ for thermal electrons and $v = c$ for relativistic electrons in Fig. 1b. The time scale of the thermal quench associated with the departure of the plasma along the field lines is found to be comparable with the thermal collision time but shorter than the collisional time scale for relativistic electrons $\tau(c)$, making the possibility of self-consistent calculation of the electron distribution function with the LUKE code in a rapid cooling event highly questionable. As a consequence of the rapid loss of the plasma, a well confined seed of runaway electrons near the magnetic axis may be all that remains from the suprathermal electron population in the post thermal quench phase. After the thermal quench the runaway electrons are in many cases well confined for seconds, in the so called runaway electron current plateau [11]. The high confinement in this phase likely implies recovery of the nested magnetic flux surfaces and the runaway electrons in the current plateau could in principle be modelled with the LUKE code until their final deconfinement at the end of the current plateau. However, since the non-Maxwellian electron distribution function after the thermal quench is unknown, the initial conditions necessary for runaway calculations are undefined.

With the restrictions of disruption modelling in mind, the objective of this work is to study the formation of runaway electrons in non-disruptive scenarios owing to the combined effect of Dreicer and avalanche with a fast solver of the electron distribution function in order to make predictions for the birth of runaway electrons in tokamak experiments. The difficult task of modelling the transient temperature and electric field found in disruptions, would require a proper description of the thermal quench with implemented radiative or convective loss mechanisms of the plasma energy including MHD instabilities. The coupling of the kinetic LUKE code with a fluid code such as JOREK [15], would be necessary for such a purpose, but is beyond the scope of this work. The kinetic modelling of the formation of runaway electrons is therefore done for non-disruptive scenarios as found in the current flattop with constant electric field and plasma temperature.

The LUKE code has previously been used for current drive and Dreicer runaway calculations. The model uses a relativistic collision operator for small angle collisions and a recently added description of the large angle (knock-on) collisions leading to the avalanche effect, which enables a description of the full

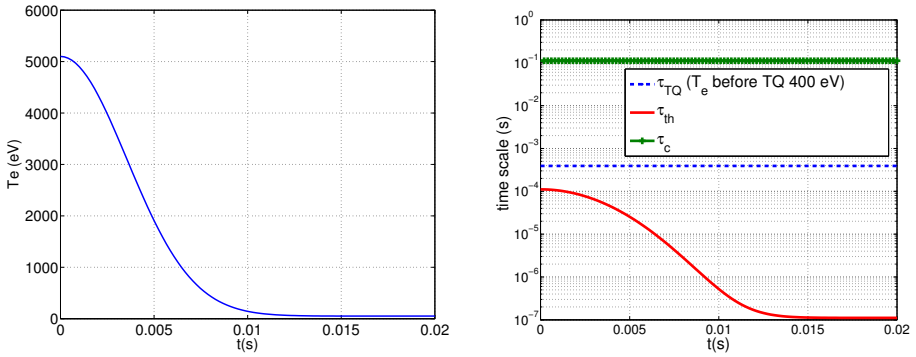

(a) (b)

Figure 1: A prescribed central temperature evolution in a thermal quench (a). Comparison of typical time scale for thermal quench with the initial temperature near the edge $T_e=400$ eV (Eq. 2) with thermal and relativistic collisional time scales (b).

2-D momentum dynamics of the runaway population. Knock-on electrons are principally scattered off with a perpendicular component of the momentum with respect to the local magnetic field direction. In a non-uniform magnetic field configuration highly magnetized electrons could be subject to magnetic trapping effects resulting in a runaway electron growth rate off the magnetic axis that differs from the estimates for a cylindric geometry. Such toroidicity effects are studied by implementing a 2-D kinetic description of the knock-on momentum dynamics, including the momentum dynamics both perpendicular and parallel to the magnetic field lines.

The knock-on collisions are included in the kinetic equation through a source term from Ref. [3], implemented along with a sink term to ensure a particle conserving form of the process. The bounce-averaged knock-on source term is presented in Sec. 2. In Sec. 3 the effect of magnetic trapping in a non-uniform magnetic field configuration is investigated. The role played by the magnetic mirror force on the runaway population off the magnetic axis, owing to a reduction in Dreicer growth rate as well as the high magnetization of the knock-on electrons, is depicted. Finally, in Sec. 4, the relative importance of the avalanche effect compared to the Dreicer mechanism is quantified as a function of plasma temperature and toroidal electric field strength. The parametric dependencies of the relative importance of the avalanche effect from the numerical modelling is related both to analytic predictions and to data from runaway observations in non-disruptive scenarios from several tokamak experiments including a low density flattop pulse from the Tore Supra tokamak, during which suprathermal electrons are observed. The analysis of this scenario supports the recently published results [14], showing that runaway electron formation requires lower

density than expected from collisional theory, which suggests the existence of additional runaway electron loss mechanisms.

2 Knock-on collisions

Knock-on collisions are considered between a relativistic electron characterized by the Lorentz factor $\gamma_1 = \sqrt{1+p_1^2}$, where p_1 is its momentum normalized to $m_0 c$ where m_0 is the electron rest mass and c the speed of light, and another electron at rest. After the collision, the secondary electron that was initially at rest has gained the momentum p_2, and $\gamma_2 = \sqrt{1+p_2^2}$ while the primary electron is assumed to remain relativistic ($p_2 \ll p_1$). Since the total momentum of the system formed by the two electrons is conserved, the secondary electron is scattered with a pitch-angle with respect to the direction of the incoming electron, whose cosine ξ^* is given by the relation

$$\xi^* = \frac{\sqrt{\gamma_1+1}\sqrt{\gamma_2-1}}{\sqrt{\gamma_1-1}\sqrt{\gamma_2+1}}. \tag{4}$$

The primary electron is assumed to be very energetic ($\gamma_1 \to \infty$) and ξ^* simplifies to

$$\xi^* = \sqrt{\frac{\gamma_2-1}{\gamma_2+1}}. \tag{5}$$

In this limit, most of the secondary electrons have a moderate kinetic energy $\gamma_2 \sim 1$. As a result of momentum conservation and the assumption that the primary electron has momentum entirely parallel to the magnetic field lines, the pitch-angle of the scattered electron will be close to $\pi/2$ with respect to the magnetic field lines. Owing to the high magnetization the electrons will be sensitive to the non-uniform magnetic field. Hence it is necessary to properly account for the 2-D guiding-center momentum dynamics in non-uniform magnetic field geometries, where the electrons are influenced by the magnetic trapping effect. The description of knock-on collisions is by definition beyond the FP approximation, which is only valid for small angle deflections that weakly modify the electron trajectories. Therefore, in order to introduce the knock-on collisions in a FP solver, it is necessary to express this process as a source term [3], that determines to where in momentum space secondary electrons are scattered, in close collisions with relativistic electrons. This source term is proportional to the relativistic electron electron differential cross section derived by Møller [16]

$$\frac{d\sigma}{d\Omega} = r_e^2 \frac{\sum(\gamma_1,\gamma_2)}{p_2\gamma_2}\delta(\xi - \xi^*(p_2)), \tag{6}$$

where

$$r_e = e^2/(4\pi\varepsilon_0 m_e c^2), \tag{7}$$

is the classical electron radius and

$$\sum(\gamma_1,\gamma_2) = \frac{\gamma_1^2}{(\gamma_1^2-1)(\gamma_2-1)^2(\gamma_1-\gamma_2)^2}\times \tag{8}$$

$$\times\Big\{(\gamma_1-1)^2-\frac{(\gamma_2-1)(\gamma_1-\gamma_2)}{\gamma_1^2}\cdot\Big[2\gamma_1^2+2\gamma_1-1-(\gamma_2-1)(\gamma_1-\gamma_2)\Big]\Big\}.$$

In the limit of a primary electron (with index '1') at velocity near the speed of light, the expression simplifies to

$$\sum_{\gamma_1\to\infty}(\gamma_1,\gamma_2)\approx\frac{1}{(\gamma_2-1)^2},$$

and the differential cross section becomes

$$\frac{d\sigma}{d\Omega}=r_e^2\frac{1}{p\gamma(\gamma-1)^2}\delta(\xi-\xi^*(p)), \tag{9}$$

where the index '2' on γ has been dropped, since the expression is now independent of γ_1 and p_1. The source term $\mathbf{S}$, originally formulated in Ref. [3], is proportional to the target population, i.e. the bulk electron density n_e. For knock-on collisions to occur, a runaway electron population n_r must exist. In the model from Ref. [3], the runaway electrons are assumed to have the speed of light (c). In this case, the source term has the form

$$\begin{aligned}\mathbf{S}(p,\psi,\xi,\theta) &= n_e(\psi)n_r(\psi)c\frac{d\sigma}{d\Omega}(p,\xi,\theta)= \\ &= n_e n_r c r_e^2\frac{1}{p\gamma(\gamma-1)^2}\delta(\xi-\xi^*(p))= \\ &= \frac{n_r}{4\pi\tau\ln\Lambda}\frac{1}{p^2}\frac{d}{dp}\Big(\frac{1}{1-\sqrt{1+p^2}}\Big)\delta(\xi-\xi^*(p))\end{aligned} \tag{10}$$

where ψ is the poloidal magnetic flux surface coordinate and θ is the poloidal angle [3]. In the above expression, the collision time for relativistic electrons

$$\tau=\frac{4\pi\varepsilon_0^2 m_e^2 c^3}{n_e e^4\ln\Lambda}, \tag{11}$$

has been introduced and $n_e c r_e^2 = 1/(4\pi\tau\ln\Lambda)$ according to Eq. 7.

2.1 Implementation of knock-on collisions in the LUKE code

An analytic estimate of the avalanche growth rate is obtained from integration of the knock-on source term in Eq. 10 over the runaway region $p > p_c$ in momentum space, as done in the work by Rosenbluth [3]

$$\frac{1}{n_r}\frac{\partial n_r}{\partial t} = \frac{1}{n_r}\int_{p_c}^{\infty}\mathbf{S}\,d^3p= \tag{12}$$

$$= \frac{1}{n_r}2\pi\int_{p_c}^{\infty}\int_{-1}^{1}\mathbf{S}\,p^2dp\,d\xi=\frac{1}{2\tau\ln\Lambda}\left[\frac{1}{1-\sqrt{1+p^2}}\right]_{p_c}^{\infty}. \tag{13}$$

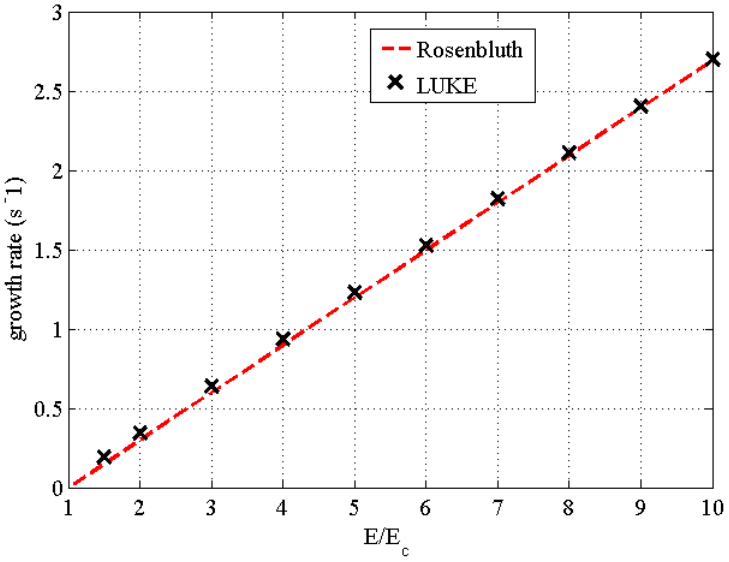

Figure 2: The knock-on process in LUKE (crosses) benchmarked against analytic growth rate in Ref. [3] (dashed line), when using the same momentum space offsets.

If $E/E_c \gg 1$ and p_c is small

$$\frac{1}{n_r}\frac{\partial n_r}{\partial t} = \frac{1}{2\tau \ln\Lambda}\left(\frac{1}{\sqrt{1+p_c^2}-1}\right) \approx \frac{1}{2\tau \ln\Lambda}\left(\frac{2}{p_c^2}\right). \tag{14}$$

With the critical momentum $p_c^2(\xi = 0) = 2E_c/E$ and adding the term -1 in the numerator to ensure that no runaway generation occurs for $E/E_c = 1$, Eq. 14 gives an analytic estimate of the growth rate [3]

$$\frac{1}{n_r}\frac{\partial n_r}{\partial t} = \frac{1}{2\tau \ln\Lambda}\left(E/E_c - 1\right). \tag{15}$$

The runaway generation through knock-on collisions in LUKE is benchmarked against the growth rate in Eq. 15 in the case of cylindrical geometry in Fig. 2, by using the same momentum offsets.

The Rosenbluth model [3] assumes that existing runaway electrons have infinite momentum, but in the numerical calculations a limit $p_{max} > p_c$ for the momentum grid must be defined. The growth rate is evaluated by LUKE as the flux of electrons through p_{re} when an electron gains enough energy to diffuse through the momentum space boundary. This value is set to $p_{re} = \max(p_c; p(E_k = 1\,\mathrm{MeV}) \approx 2\sqrt{2}p_{th})$ to account for the primary runaway electrons with kinetic energy above 1 MeV. With $v/c \geq 0.94$, corresponding to $E_k \geq 1$

MeV, this criterion is close to the assumptions in Ref. [3] and is further justified by the weak dependence of the knock-on source term upon the incident electron energy in the energy range $1 - 100\,\mathrm{MeV}$ [17].

The bulk electron density is defined as the integral of the bulk electron distribution in momentum space:

$$\int_0^{p_{re}} f(r,p) d^3p = n_e(r) \tag{16}$$

The bulk and the runaway region, corresponding to $p < p_{re}$ and $p > p_{re}$ respectively, are shown in Fig. 3. The runaway electron population is defined as

$$n_r(t) = \int_0^t \left(\gamma_D + \int_{p_{re}}^{p_{max}} S\, d^3p \right) dt,$$

where $\gamma_D = \iint \mathbf{S_p}(\psi, p, \xi) \cdot d\mathbf{S}$ is the integral of the particle flux through the surface element $d\mathbf{S} = p_{re}^2 d\xi d\varphi \hat{\varphi}$. In order to ensure conservation of number of particles in LUKE, as electrons enter the runaway momentum region, i.e. diffuse through p_{re} either from the Dreicer mechanism or by knock-on collisions, the same amount of electrons are removed from the bulk. A sink term accounting for the electrons transported from bulk to runaway momentum region is added along with the source term. The particle conserving knock-on process takes the form:

$$\mathbf{S} = \mathbf{S}_+ - < \mathbf{S}_+ > \frac{f_M}{< f_M >}, \tag{17}$$

where f_M is the bulk distribution, assumed to be Maxwellian and $< ... >= \int_0^{p_{max}} ... d^3p$. The source and sink terms conserve the number of electrons $n_e + n_r = n_{tot} = const.$.

2.2 Runaway electron growth rate

The runaway electron model implemented in LUKE captures the combined effect of Dreicer and avalanche generation. The evolution of the runaway electron population under the influence of a constant electric field is calculated, including the effect of the avalanche mechanism due to knock-on collisions. Figure 4 shows the evolution of a runaway electron fraction with and without the knock-on driven avalanche effect. At first, there are very few runaway electrons, the avalanche contribution becomes significant only when a runaway electron population has been built up by the Dreicer effect. Then, the avalanche due to knock-on collisions leads to exponential growth of the runaway electron population and quickly becomes dominant over the Dreicer generation.

Both the Dreicer and avalanche mechanisms are proportional to the bulk density $n_e = n_{tot} - n_r$, such that the runaway production rate can be expressed in the generic form

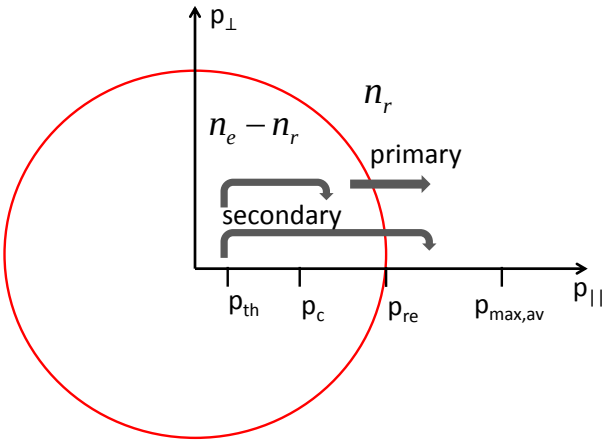

Figure 3: The LUKE momentum space is divided into two separate populations: the bulk electrons with momentum $p < p_{re}$ and the runaway electrons $p > p_{re}$. The knock-on collisions between the populations n_r and n_e can lead to secondary runaway electrons. Electrons that escape the domain $p < p_{re}$ either by electrons diffusing through p_{re} or by getting directly knocked into the runaway region at $p > p_{re}$ contribute to the runaway electron population n_r.

$$\frac{\partial n_r}{\partial t} = n_e \left(\gamma_D + \gamma_A\right) \rightarrow \frac{1}{(n_{tot} - n_r)} \frac{\partial n_r}{\partial t} = \gamma_D + \gamma_A. \tag{18}$$

To quantify the avalanche growth rate, the avalanche term may be expressed as $\gamma_A = n_r \bar{\gamma}_A$, where $\bar{\gamma}_A$ is an avalanche multiplication factor. Thus, Eq. 18 becomes:

$$\frac{1}{(n_{tot} - n_r)} \frac{\partial n_r}{\partial t} = \gamma_D + n_r \bar{\gamma}_A. \tag{19}$$

Equation 19 is a function of $n_r(t)$, where the constant term is the Dreicer growth rate and the avalanche multiplication factor is given by the slope. In Fig. 5 the growth rate given by Eq. 18 is illustrated for $E/E_c = 40$ and 60 and $T_e = 0.5$ keV. The growth rates from the LUKE calculations are evaluated numerically, the Dreicer as a constant value (γ_D) and the avalanche multiplication factor ($\bar{\gamma}_A$) from the slope of the curve. The Dreicer growth rate calculated by LUKE agrees well with predictions of the Kulsrud model (Ref. [18]) where the Fokker Planck equation is solved numerically. The Dreicer growth rate γ_D is not directly comparable to the avalanche factor $\bar{\gamma}_A$, as the latter is normalized to the runaway electron density and it is rather a factor depending on the electric field and the plasma density. The avalanche multiplication factor $\bar{\gamma}_A$ characterizes the tendency of a runaway avalanche to develop, for a given magnetic equilibrium and parallel electric field. The actual runaway production due to avalanche is however time dependent since it is a product of the avalanche multiplication factor $\bar{\gamma}_A$ and the time dependent runaway electron density n_r. For example, $\bar{\gamma}_A$ can be non-zero, even though the number of runaway electrons born from knock-on collisions is negligible, if no seed of primary electrons is formed first.

The avalanche theory in Ref. [3] assumes that all electrons with momentum larger than p_c will run away. With the LUKE code, it is possible to go beyond this estimate, for a more realistic description of the runaway electron distribution function by also including the treatment of secondary electrons with momentum in the collisional momentum region $p < p_c$. Indeed these electrons that are not in the momentum space runaway region could contribute to the hot tail formation. Since the knock-on collisions also accelerate electrons to intermediate energies $p_{th} < p < p_c$, it is in principle important to include all electrons with $p > p_{th}$. However, it is found that the inclusion of the knock-on electrons in the suprathermal region has a negligible effect on the growth rate in the simulations done in this work, as is shown in Fig. 6, where the contribution to the avalanche growth rate in the momentum region $p_{th} < p < p_c$ is negligible. It should however be pointed out that these calculations are done for constant electric field and the treatment of the knock-on born electrons near the runaway region could be crucial in a transient electric field where the boundary between the runaway momentum region and the collisional region varies in time.

The avalanche theory by Rosenbluth's model accounts for runaway electrons born due to knock-on collisions in momentum space in the interval $[p_c, \infty]$. In

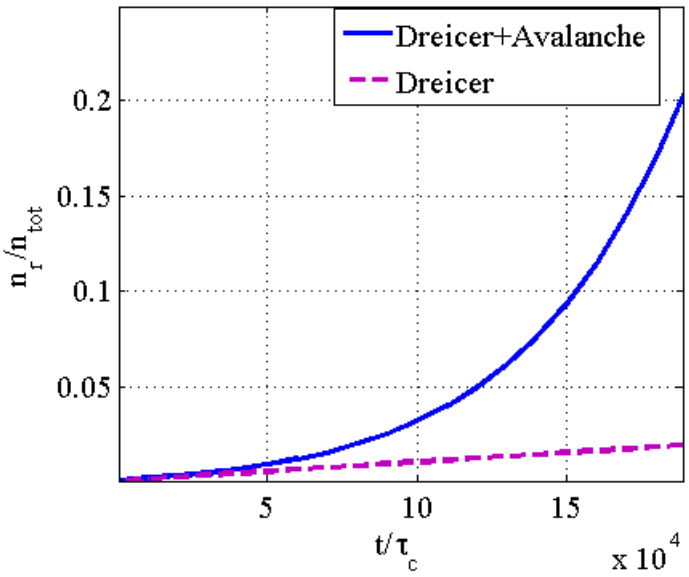

Figure 4: The fraction of runaway electrons ($E/E_c = 30$ and $T_e = 0.5$ keV) as a function of time normalized to thermal collision time, with and without the avalanche effect due to the knock-on collisions. .

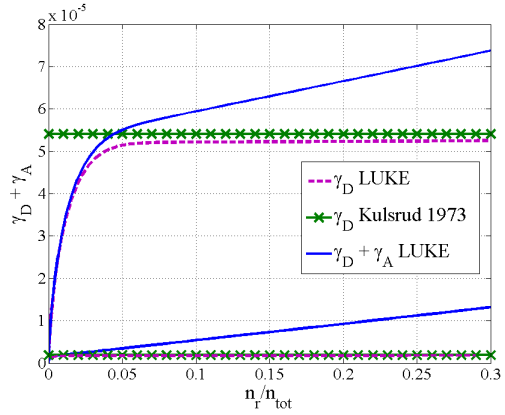

Figure 5: The growth rate in constant electric field and $T_e = 0.5$ keV for $E/E_c = 40$ (the curves with lower growth rate) and $E/E_c = 60$ (curves with higher growth rate) as a function of the runaway electron density, with and without the avalanche effect. The Dreicer contribution is in good agreement with Kulsrud's theory [18]. The growth rates are normalized to the thermal collision frequency ($\nu_{th} = 1/\tau(v_{th})$)

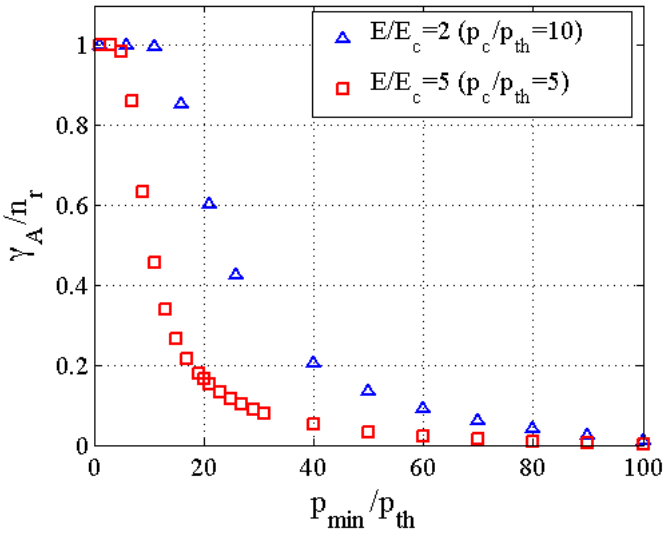

Figure 6: Avalanche multiplication factor as a function of the lower momentum cut off p_{min}/p_{th} for $T_e = 5$ keV, normalized to the avalanche factor at $p_{min} = p_c$.

the treatment of the secondary runaway electrons due to knock-on collisions in LUKE, a finite upper limit p_{max} must be chosen above which the contribution to the runaway population is neglected (see Fig. 3). The knock-on production decreases with momentum, with the knock-on source term (Eq. 10) $\mathbf{S} \to 0$ for $p \to \infty$. In LUKE p_{max} has to be defined at large enough momentum to account for the dominant part of the knock-on collision contribution. The avalanche multiplication factor ($\bar{\gamma}_A$) as a function of a lower cutoff (p_{min}) for the population of secondary electrons has been computed in order to quantify at what value the avalanche production gets negligible. It is found that most contribution to the avalanche factor originates from the knock-on electrons born near the critical momentum p_c. In Fig. 6 the avalanche factor for different momentum intervals is shown, for electric field $E/E_c = 2$ and $E/E_c = 5$ ($T_e = 5$ keV). The calculations provide an estimate of the minimum momentum interval needed to include the dominant part of the avalanche production. To capture 80% of the avalanche physics, the source term must be accounted for up to at least $p_{max,av} = 4 \cdot p_c$.

2.3 Bounce-averaged knock-on source term

Since knock-on accelerated electrons emerge with high perpendicular momentum [3], it is necessary to properly account for the guiding-center dynamics in non-uniform magnetic field geometry and treat the full 2-D momentum electron dynamics. The knock-on source term presented in Eq. 10 is 4-dimensional

(p, ψ, ξ, θ) but by averaging over the poloidal motion the dimensionality gets reduced to 3-D (p, ψ, ξ_0) such that the dynamics is projected onto the poloidal position θ_0 of the minimum magnetic field $B_0(\psi)$ on a magnetic flux surface. Bounce-average is valid when the collisional time is longer than the bounce period [2]. The bounce-averaged knock-on source term is

$$\{\mathbf{S}\}(\psi, p, \xi_0) = \frac{1}{\lambda \widetilde{q}} \left[\frac{1}{2}\sum_{\sigma}\right]_T \int_{\theta_{min}}^{\theta_{max}} \frac{d\theta}{2\pi} \frac{1}{|\hat{\psi}\cdot\hat{r}|} \frac{r}{R_p}\frac{B}{B_p}\frac{\xi_0}{\xi}\mathbf{S}(\psi, p, \xi). \tag{20}$$

where R_p is the major radius, θ_{min} and θ_{max} are the poloidal turning points for the trapped electrons, B_p is the poloidal component of the magnetic field B and the sum over σ applies to trapped particles (T) only. The normalized bounce time is

$$\lambda(\psi) = \frac{1}{\widetilde{q}(\psi)} \int_{\theta_{min}}^{\theta_{max}} \frac{d\theta}{2\pi} \frac{1}{|\hat{\psi}\cdot\hat{r}|} \frac{r}{R_p}\frac{\xi_0}{\xi}\frac{B}{B_p},$$

and

$$\widetilde{q}(\psi) \equiv \int_0^{2\pi} \frac{d\theta}{2\pi} \frac{1}{|\hat{\psi}\cdot\hat{r}|} \frac{r}{R_p}\frac{B}{B_p}.$$

In the LUKE code, the terms in the Fokker-Planck equation are normalized to a reference density $n_e^\dagger$ and the reference thermal collision frequency $\nu_{coll}^\dagger = 1/\tau(v_{th})$, so that the implemented source term is $\bar{\mathbf{S}} = \mathbf{S}/\mathbf{S}^\dagger$ where $\mathbf{S}$ is from Eq. 10 and $\mathbf{S}^\dagger = n_e^\dagger \nu_{coll}^\dagger$ and the momentum is normalized to the thermal momentum $\bar{p} = p/p_{th}$. The knock-on source term is decomposed as $\bar{\mathbf{S}}(p, \psi, \xi, \theta) = \bar{\mathbf{S}}^* \delta(\xi - \xi^*(\bar{p}))$ where

$$\bar{\mathbf{S}}^* = \frac{1}{4\pi}\frac{\beta_{th}^{\dagger 2}}{\ln\Lambda^\dagger}\bar{n}_e\bar{n}_r\frac{1}{\bar{p}\gamma(\gamma-1)^2}, \tag{21}$$

is independent of θ, so that $\{\bar{\mathbf{S}}\} = \bar{\mathbf{S}}^*\{\delta(\xi - \xi^*(\bar{p}))\}$ where ξ is the pitch angle cosine at the poloidal angle position θ

$$\xi = \sigma\sqrt{1 - \Psi(\psi, \theta)(1 - \xi_0^2)}. \tag{22}$$

Here $\Psi(\psi, \theta) = B(\psi, \theta)/B_0(\psi)$ and $\sigma = sign(v_{||}) = sign(\xi_0)$ indicates the direction of the electrons along the magnetic field line. Using the general relation for Dirac's delta function $\delta(g(x)) = \sum_k \delta(x - x_k)/|g'(x_k)|$ where x_k are the zeros of the function $g(x)$ and $g'(x) = dg/dx$ provided that $g(x)$ is a continuously differentiable function and $g'(x)$ is non-zero:

$$\delta(\xi - \xi^*) = \sum_k \frac{2\delta(\theta - \theta_k^*)|\xi^*|}{|\Psi'(\psi, \theta_k^*)|(1 - \xi_0^2)}, \tag{23}$$

where θ_k^* is the poloidal angle at which the secondary electron emerges. From Eq. 22 θ_k^* is given by,

$$\sigma\sqrt{1-\Psi(\psi,\theta_k^*)(1-\xi_0^2)}-\xi^*=0 \tag{24}$$

or

$$\Psi(\psi,\theta_k^*)=\frac{B_{\theta_k^*}}{B_0}=\frac{1-\xi^{*2}}{1-\xi_0^2}=\frac{2}{(1-\xi_0^2)(\gamma+1)}. \tag{25}$$

Using Eq. 23, the delta function can be expressed as

$$\{\delta(\xi-\xi^*)\}=\frac{1}{\lambda\widetilde{q}}\frac{1}{\pi}\sum_k\frac{1}{|\hat{\psi}\cdot\hat{r}|_{\theta_k^*}}\frac{r_{\theta_k^*}}{R_p}\frac{B_{\theta_k^*}}{B_{p,\theta_k^*}}\frac{\xi_0}{\xi_{\theta_k^*}}\frac{|\xi^*|}{|\Psi'(\psi,\theta_k^*)|(1-\xi_0^2)}.$$

and since $B_{\theta_k^*}=(1-\xi^{*2})/(1-\xi_0^2)B_0$ with $\xi_{\theta_k^*}=\xi^*$

$$\{\delta(\xi-\xi^*)\}=\frac{1}{\lambda\widetilde{q}}\frac{1}{\pi}\sum_k\frac{1}{|\hat{\psi}\cdot\hat{r}|_{\theta_k^*}}\frac{r_{\theta_k^*}}{R_p}\frac{B_0}{B_{p,\theta_k^*}}|\xi_0|\frac{(1-\xi^{*2})}{|\Psi'(\psi,\theta_k^*)|(1-\xi_0^2)^2}, \tag{26}$$

and the normalized, bounce-averaged avalanche operator becomes

$$\begin{aligned}\{\bar{\mathbf{S}}\} &= = \frac{1}{2\pi^2}\frac{\beta_{th}^{\dagger 2}}{\ln\Lambda^\dagger R_p}\bar{n}_e\bar{n}_r\cdot \\ &\frac{1}{\bar{p}\gamma(\gamma-1)^2(\gamma+1)}\frac{B_0}{\lambda\widetilde{q}}\frac{|\xi_0|}{(1-\xi_0^2)^2}\sum_k\Big[\frac{1}{|\hat{\psi}\cdot\hat{r}|_{\theta_k^*}}\frac{r_{\theta_k^*}}{B_{p,\theta_k^*}}\frac{1}{|\Psi'(\psi,\theta_k^*)|}\Big]\end{aligned} \tag{27}$$

which can be expressed as:

$$\begin{aligned}\{\bar{\mathbf{S}}(p,\psi,\xi_0)\} &= \frac{1}{2\pi^2}\frac{1}{\ln\Lambda^\dagger R_p}\bar{n}_e\bar{n}_r\cdot \\ &\frac{1}{\bar{p}^3\gamma(\gamma-1)}\frac{B_0}{\lambda\widetilde{q}}\frac{|\xi_0|}{(1-\xi_0^2)^2}\sum_k\Big[\frac{1}{|\hat{\psi}\cdot\hat{r}|}\frac{r}{B_p}\frac{1}{|\Psi'|}\Big]_{\theta_k^*},\end{aligned} \tag{28}$$

using the relation $p^2=(\gamma^2-1)=(\gamma-1)(\gamma+1)$ and $p=\bar{p}\beta_{th}$,

3 Effect of toroidicity

The bounce-averaged treatment of the calculations in LUKE, including the bounce-averaged knock-on source term in Eq. 28, allows for investigation of the effect of a toroidal magnetic field configuration on the evolution of the runaway electron population. Owing to magnetic mirror effects off the magnetic axis, the generation of runaway electrons may be expected to reduce, since the velocity of a trapped electron is bounded as it goes to zero at its turning points in the banana orbit. Such a radial dependence is not included in Kulsrud's model [18]. However, the effect has previously been identified numerically for Dreicer runaway generation [2, 19]. The growth rate presented in Sec. 2.2 obtained

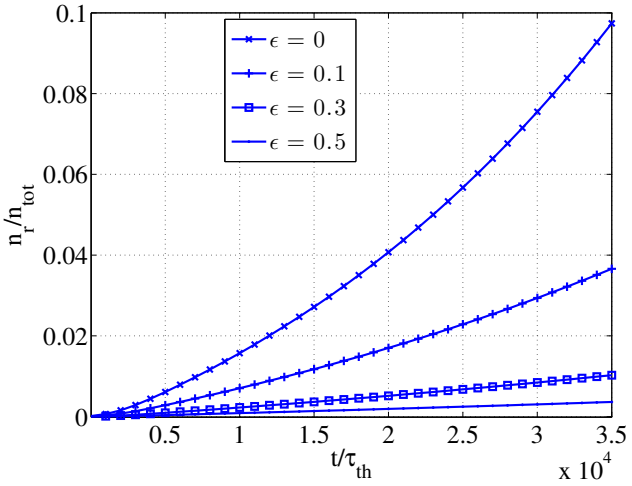

Figure 7: The evolution of the runaway electron population, including the avalanche effect owing to knock-on collisions, depends strongly on the radial position in a non-uniform magnetic field configuration, where $\epsilon = r/R$ is the inverse aspect ratio coordinate. $E/E_c = 40$, $T_e = 0.5$ keV and the time t is normalized to the thermal collision time τ_{th}.

with the knock-on source term in Eq. 10 is valid in the cylindrical limit as well as on the magnetic axis, where magnetic trapping is negligible. The trapping effect is considered as a correction to the growth rate in Eq. 15, for which the significance increases away from the magnetic axis as the fraction of trapped electrons becomes larger. As discussed in Sec. 2, secondary electrons emerging from the knock-on collisions are highly magnetized. Since the trapping effect increases off the magnetic axis in a non-uniform magnetic field configuration, the further away from the magnetic axis the electrons appear, the more they tend to be born trapped [3]. These trapped electrons may eventually untrap due to pitch angle scattering, but the growth rate could at least momentaneously get reduced.

To quantify the tendency of magnetic trapping, the bounce-averaged calculations of the runaway electron population are performed in a scenario with circular plasma cross section and high magnetic non-uniformity, with inverse aspect ratio ranging from $\epsilon = 0$ to $\epsilon = a/R = 1$. The inverse aspect ratio of the Tore Supra tokamak is $\epsilon \approx 0.3$. The calculations in Fig. 7 reveal that the runaway electron population grows significantly slower off the magnetic axis than in the center. This result suggest that runaway electrons appear near the magnetic axis rather than near the edge.

In order to study the trapping effects on the runaway population, the Dreicer growth rate γ_D and the avalanche multiplication factor $\bar{\gamma}_A$ are quantified separately. The Dreicer growth rate is found to be strongly affected by the non-

uniformity of the magnetic field, as shown in Fig. 8. A fit of the numerical results gives an analytic expression of the Dreicer growth rate $\gamma_D = 1 - \sqrt{2\epsilon/(1+\epsilon)}$. The results indicate that for $\epsilon > 0.5$ runaway generation from Dreicer acceleration is nearly canceled.

For the runaway electrons generated from knock-on collisions, the avalanche multiplication factor $\bar{\gamma}_A$ may be expected to be reduced by magnetic trapping due to a non-uniform magnetic configuration since the knock-on electrons are highly magnetized and therefore sensitive to magnetic field variations. The avalanche runaway production, being directly proportional to the existing runaway electron population, will in addition be suppressed from the particle trapping effect on Dreicer generation that leads to a reduced seed n_r, as presented in Fig. 8. The reduction of $\bar{\gamma}_A$ obtained from bounce-averaged calculations with LUKE off the magnetic axis is shown in Fig. 9, with an avalanche multiplication factor that decreases with the inverse aspect ratio. This means that there is a reduction, independent of the seed term itself, of the avalanche runaway rate off the magnetic axis. In order to validate the radial dependence of the avalanche factor obtained from the LUKE simulations, an analytical estimate for avalanche growth rate including the effect of magnetic trapping due to a non uniform magnetic configuration is derived. It is based on the assumption that all electrons with momentum $p > p_c$ will contribute to the runaway population (as in Ref. [3]), except the secondary electrons that appear in the trapped momentum region $p < p_T$. The magnetic trapping criterion is obtained from the condition

$$\frac{B(\theta)}{B_{max}} > \frac{2}{\sqrt{1+p^2}+1}, \tag{29}$$

where $B_{max}/B(\theta) = (1+\epsilon\cos\theta)/(1-\epsilon)$ in a circular concentric magnetic configuration. Electrons will run away if their momentum exceeds both the critical momentum and the trapping condition in Eq. 29 and the lower integration limit p_{min} for the analytical estimate of the avalanche growth rate is given by $max(p_c, p_T)$. An analytical expression for the inverse aspect ratio dependent avalanche growth rate is obtained by integrating the source term from over momentum space from $p_{min} = \max(p_c(E/E_c), p_T(\theta))$ to $p_{max} = \infty$ where

$$\begin{aligned} p_T^2 &= \left(2B_{max}/B(\theta) - 1\right)^2 - 1 \quad = \\ &\approx 4\epsilon(1+cos\theta)/(1-\epsilon)^2 \end{aligned} \tag{30}$$

and

$$p_c^2 = 2E_c/E$$

This results in a locally modified, inverse aspect ratio dependent avalanche growth rate

$$\frac{dn_r}{dt_n}(\theta,\epsilon) \quad = \quad \frac{1}{2}\frac{1}{\ln\Lambda^\dagger}\bar{n}_e\bar{n}_r\frac{1}{\sqrt{1+p_{min}^2}-1} =$$

$$= \frac{1}{2}\frac{1}{\ln\Lambda^{\dagger}}\bar{n}_e\bar{n}_r \,\mathsf{min}\left(\frac{E}{E_c}, \frac{(1-\epsilon)^2}{2\epsilon(1+cos\theta)}\right). \qquad (31)$$

The flux surface averaged growth rate is derived in Appendix A. For $\epsilon E/E_c \gg 1$, $\theta_b \to \pi$, the growth rate is reduced by a factor $(1-\epsilon)^2/\left(\pi\sqrt{\epsilon E/E_c}\right)$. The inverse aspect ratio dependence of the estimated avalanche growth rate obtained from Eq. 31 is compared to numerical results. Numerical integration of the source term is also performed, with the same criterion on the lower integration boundary in momentum space p_{min} as the analytic estimate in Eq. 36 . The analytic result is also compared to avalanche growth rate from Fokker-Planck calculations with the LUKE code. In that case, the trapping conditions are the same as in the analytic result, except for that the critical momentum is pitch angle dependent $p_c^2 = E_c/(E\xi)$. The LUKE calculated avalanche multiplication factor and the analytical estimate show good agreement (Fig. 9).

Figure 9 shows the reduced growth rate for $E/E_c = 5$, relative to a cylindric plasma, equivalent to the growth rate on the magnetic axis ($\epsilon = 0$). Numerical integration of the source term shows good agreement with the analytic result (Eq. 36). Close to the center, at low inverse aspect ratio, the effect of trapping is not visible, since the critical momentum is higher than the trapped momentum over the whole flux surface. This effect decreases with increasing E/E_c as the critical momentum p_c decreases and becomes less restrictive compared to the trapping condition p_T, which explains the flat top seen in Fig. 9. However, for the FP calculations the magnetic trapping effect influences the growth rate also close to the magnetic axis. A possible explanation is pitch angle collisions that couple the dynamics between the trapped and the passing region.

The growth rate obtained from bounce-averaged calculations suggest that the formation of runaway electrons is slower the further away from the magnetic axis they appear. In other words, the time scale of the local growth rate could be longer than suggested by collisional theory [18, 3]. Potential loss mechanisms, such as transport of fast electrons due to magnetic field perturbations [20] could therefore act more efficiently on the runaway electrons formed off the magnetic axis than the ones formed on axis which could lead to well confined runaway electrons at the center of the plasma.

4 The relative importance of the avalanche effect

The results presented in Sec. 2.2 (see Fig. 4) have shown that the runaway electron distribution can be significantly modified by including the effect of knock-on collisions. In order to understand the mechanisms that govern the runaway electron generation processes a parametric study is performed with the aim to investigate which runaway formation process; Dreicer or avalanche, that dominates in non-disruptive tokamak experiments.

The relative importance of the avalanche mechanism to the Dreicer mechanism can be estimated by comparing the analytic avalanche growth rate in Eq. 15 and the Dreicer generation that is derived in Ref. [7]:

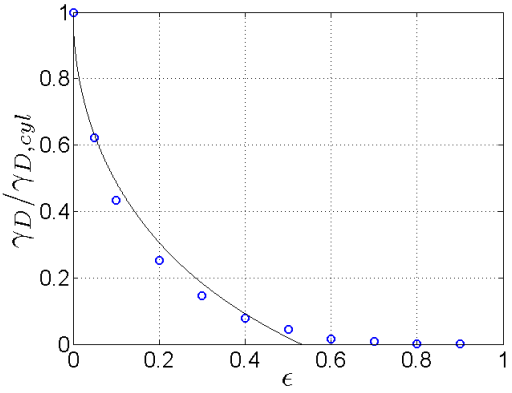

Figure 8: Radial dependence of Dreicer growth rate, normalized to the growth rate for cylindrical case $\epsilon = 0$ and a fit $\gamma_D/\gamma_{D,cyl} = 1 - 1.2\sqrt{2\epsilon/(1+\epsilon)}$.

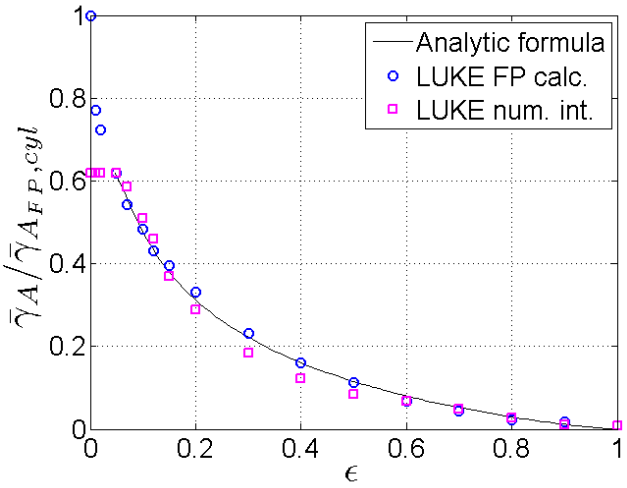

Figure 9: Radial dependence of the avalanche multiplication factor from bounce-averaged LUKE calculations (circles), normalized to to the avalanche multiplication factor for the cylindrical case $\epsilon = 0$. The numerical integration over the knock-on source term in Eq. 10 with the toroidal dependence in the momentum integration boundary from Eq. 30 is plotted in squares. The solid line shows the analytic estimate of the growth rate off the magnetic axis from Eq. 36.

$$\left(\frac{\partial n_r}{\partial t}\right)_D \sim \frac{2}{\sqrt{\pi}} n_e \nu(v_{th}) \left(\frac{E}{E_D}\right)^{1/2} \exp\left(-\frac{E_D}{4E} - \left(\frac{2E_D}{E}\right)^{1/2}\right),$$

where $E_D = (c/v_{th})^2 E_c$ is the electric field at which even thermal electrons will run away, known as the Dreicer field. The ratio of the two growth rates is

$$\left(\tfrac{\partial n_r}{\partial t}\right)_A / \left(\tfrac{\partial n_r}{\partial t}\right)_D = \frac{\gamma_A}{\gamma_D} \sim$$
$$\sim \frac{\sqrt{\pi}}{4} \frac{n_r}{n_e} \frac{1}{\ln\Lambda} \left(\frac{v_{th}}{c}\right)^3 \left(\frac{E}{E_c} - 1\right) \left(\frac{E}{E_D}\right)^{-1/2} \exp\left(\frac{E_D}{4E_D} + \sqrt{\frac{2E_D}{E}}\right) \quad (32)$$

By letting a small fraction of electrons run away in LUKE, the relative importance of the avalanche effect as a function of plasma temperature and electric field strength can be evaluated numerically from the fraction of the runaway electrons that originate from Dreicer and knock-on collisions. In Fig. 10 the fraction of runaway electrons born from knock-on collisions is shown, when 1% of the initial electron population has run away in a cylindrical magnetic configuration with constant electric field, density and temperature. The fraction of runaway electrons has to be small enough for the equilibrium parameters to remain constant and to consider the current as driven by two separate populations; the bulk and the runaway tail. The relative importance of secondary runaway electrons grows at lower temperature and electric field, as the slower primary generation in high collisionality (low temperature) allows for runaway avalanches to take off. The duration of the electric field required to reach the runaway fraction varies strongly in the parameter space presented in Fig. 10. The time required for 1% of the electrons to run away is illustrated for various electron temperatures (T_e = 0.05, 0.5, 2 and 5 keV) in Fig. 11. The formation of runaway electrons slows down as the collisionality increases at lower bulk temperature.

The numerical results are compared with the analytical estimate from Eq. 32 with $n_r/n_e = 0.01$. The condition for the dominance of the avalanche effect $\gamma_A/\gamma_D > 1$ is plotted in Fig. 10 along with the boundaries for which n_A/n_r = 5% and 90%.

In order to relate the study to experimental tokamak scenarios, it must be noted that the simulations are performed for constant electric field and temperature. Consequently, the study is restricted to non-disruptive scenarios with well-diagnosed and quiescent conditions from several tokamaks, where runaway electrons have been observed in the current flattop with the relevant plasma parameters maintained essentially constant. Results from scenarios with reproducible measurements of electron density, loop voltage and plasma temperature at the runaway electron onset from DIII-D, FTU, TEXTOR, Alcator C-Mod and KSTAR were recently published in Ref. [14]. From this study the threshold electric field normalized to the critical field is found to be significantly higher than

predicted by collisional theory where the birth of runaway electrons is predicted at $E/E_c > 1$, provided that no additional runaway electron loss mechanisms are present [18]. However, the condition for runaway onset in collisional theory does not take the time required to generate runaway electrons into account. Estimations from LUKE calculations in Fig. 11 shows that this time scale can be unrealistically large as compared to the tokamak discharge duration. The time to generate a small fraction of runaway electrons from a Maxwellian distribution is finite for $E/E_c > 1$ but as $E/E_c \to 1$, the required time to generate runaway electrons $t \to \infty$. However, it is not the only explanation since the study in Ref. [14] found that the E/E_c threshold for suppression was also well above unity.

Runaway electrons have been generated in the Tore Supra (TS) tokamak in low density discharges ($n_e < 10^{19}\ m^{-3}$). The TS pulses #40719 and #40721 are performed after a boronization and suprathermal electrons are observed in the former discharge but not in the latter. Both are Ohmic discharges at $I_p = 0.6$ MA in the current flattop. Suprathermal electrons are observed in #40719 by the ECE edge chords at current ramp-up and ramp-down, when the density is low ($< n_e >= 0.4 \cdot 10^{19}\ m^{-3}$), see Fig. 12a. The uniform E-field, estimated as the time derivative of the resistive flux [21], is $E_{\|} = 0.038 \pm 0.003$ V/m and the core temperature is 3.8 keV. The determination of the magnetic flux at the plasma boundary is described in Ref. [22]. No suprathermal electrons are detected by electron cyclotron emission (ECE) in the following pulse #40721 at a higher electron density, see Fig. 12b. Similar result is found from HXR measurements from the vertical camera detecting emission of $20 - 200$ keV (Fig. 13). A peak of photo-neutrons is observed at the plasma termination for the lower density shot (#40719) but not for the higher density shot (#40721). From the combined observations on ECE, HXR and photo-neutron measurements, the presence of relativistic electrons during the ramp-down of #40719 is identified. During the current flattop of #40719, the electron density is $< n_e >= 0.64 \cdot 10^{19}$ m^{-3}, corresponding to $E/E_c \approx 8$, but there is no sign of suprathermals until $E/E_c \approx 11$. The suprathermal generation in #40719 is added to the $(E/E_c, T_e)$ scan (see Fig. 10) and lands in the region where Dreicer generation is dominant. In the higher density pulse (#40721) $E/E_c \approx 4$ during the current flattop and no suprathermal electrons are detected. These results are in line with those of Ref. [14] where $E/E_c \sim 3 - 12$ is required to generate a detectable population of runaway electrons in the various tokamaks.

Relating the data from the experiments in Ref. [14] and the TS discharge #40719 to the parameter scan done in LUKE (Fig. 10) reveals that the scenarios fall in or close to the region where the avalanche mechanism becomes significant for the runaway electron growth rate (Fig. 10). Data from two COMPASS discharges where runaways were observed (#8555 and #8630) fall in the region where the Dreicer effect is dominant[23]. Runaway electrons are commonly produced in the current ramp-up phase of the COMPASS tokamak, due to the relatively high E/E_c ratio $(20 - 200)$. The circular 130 kA discharge #8555 was part of the electron density $< n_e >$ scan from $1 - 4 \cdot 10^{19}\ m^{-3}$, where $< n_e >$ for this particular shot was $2 \cdot 10^{19}\ m^{-3}$ during the flattop. The raise of runaway activity was observed with HXR NaI(Tl) scintillator and photoneutron

detector as the $< n_e >$ decreased from discharge to discharge, while Parail-Pogutse instability appeared for all discharges with <ne> lower than in the discharge #8555. D-shaped 160kA discharge #8630 was done for the purpose of the sawteeth-runaway correlation studies with the electron density $< n_e >= 9 \cdot 10^{19}\ m^{-3}$. Even though, the discharge had relatively high $< n_e >$, the runaway activity correlated with the sawteeth instability was visible in HXR and photoneutron signals. These two COMPASS discharges #8555 and #8630 are plotted on Fig. 10, where E/E_c at the ramp-up phase were 85 and 94, respectively. The electron density at the time of the runaway detection is $n_e =$ 1.1 and 0.80 m^{-3}. In COMPASS, interferometry is used for the line averaged electron density $< n_e >$ measurements, while Thomson scattering is used for electron temperature T_e and electron density n_e profile measurements.

These observations suggest that knock-on collisions are crucial in the formation of runaway electron generation in tokamak plasmas, even in non-disruptive scenarios. The study predicts that avalanches play an important role during current flattop. A self consistent electric field and equilibrium solver would be necessary to study avalanches with LUKE in disruptions, but is beyond the scope of the current work.

5 Conclusion

In this work the birth of runaway electrons through the combined effect of Dreicer and avalanche mechanisms is studied. Runaway avalanches are described with a knock-on source term from the work of Rosenbluth [3], implemented as a bounce-averaged conservative source/sink term within the kinetic equation in the 3-D Fokker-Planck solver LUKE. Dependencies of key parameters such as electric field strength, electron temperature and density are investigated. In addition magnetic trapping effects are quantified in a non-uniform magnetic equilibrium, resulting in a reduced runaway population off the magnetic axis for both the Dreicer and the avalanche mechanism.

The kinetic modelling of the formation of runaway electrons is restricted to non-disruptive scenarios as found in the current flattop with non-transient electric field and plasma temperature. In the LUKE code the magnetic flux surfaces are assumed to remain circular and concentric throughout the runaway formation process. The difficult task of modelling the transient temperature and electric field found in disruptions would require a proper description of the thermal quench with implemented radiative or convective loss mechanisms of the plasma energy including MHD instabilities. The coupling of the kinetic LUKE code with a fluid code such as JOREK [15] would be necessary for such a purpose, but is beyond the scope of this work. At the present, the model in which the flux surfaces are assumed to remain intact during the runaway formation can be considered as an upper estimate of the runaway formation, since possible additional losses from magnetic field stochastization that may reduce the confinement of the electrons are neglected.

Since knock-on accelerated electrons emerge with high perpendicular mo-

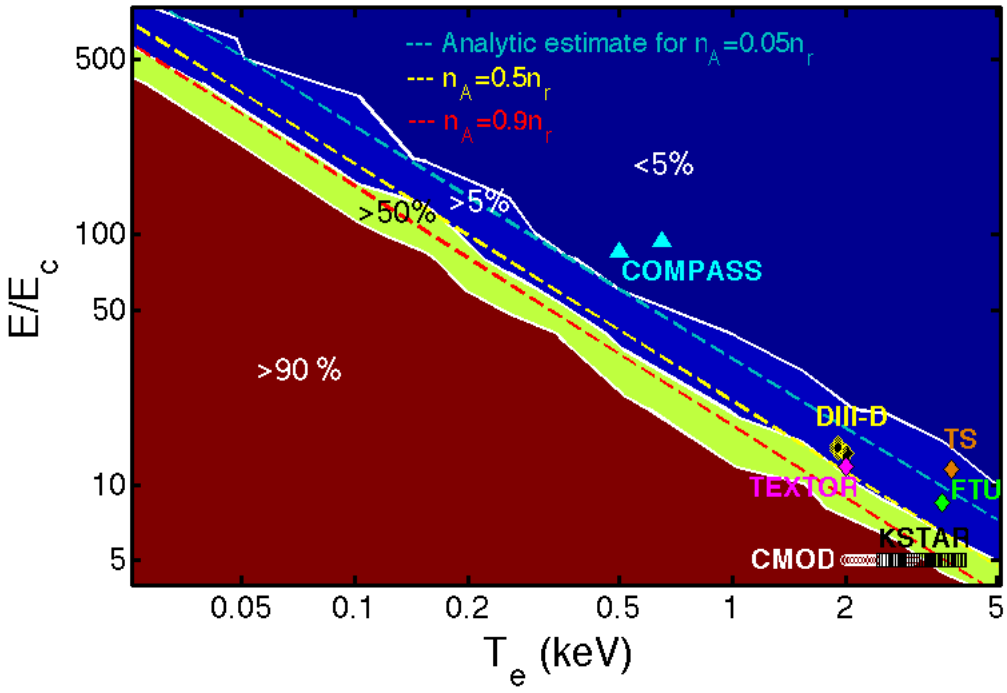

Figure 10: The fraction of runaways originating from knock-on collisions (n_A/n_r) as modelled in LUKE. The analytic estimate of when 5% (cyan line), 50% (yellow line) and 90% (red line) of the runaways come from avalanche is obtained from Eq. 32. Relation to non-disruptive scenarios where runaway electrons where generated in several tokamaks. All data points are taken from Ref. [14] except for the Tore Supra (TS) point and COMPASS points (discharge #8555 and #8630).

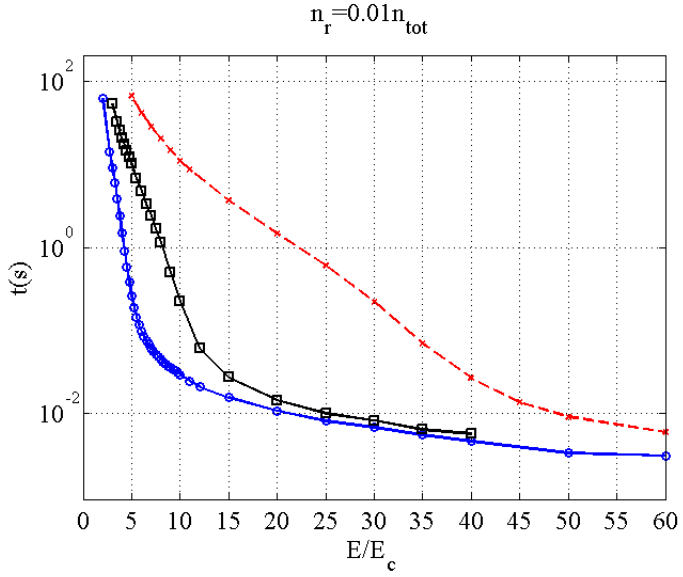

Figure 11: The time required for 1% of the Maxwellian electrons to run away, for the electron temperature $T_e = 0.5$ keV (dashed line), 2 keV (solid line and squares) and 5 keV (solid line and circles) .

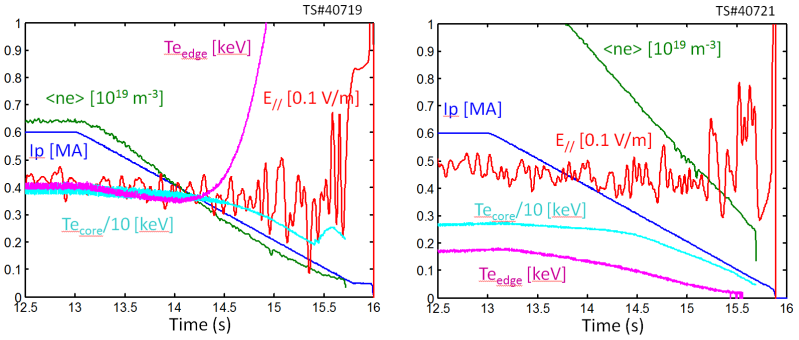

(a) (b)

Figure 12: Signature of suprathermal electrons on the edge ECE chord at around $t = 14.5$ s are seen in the Tore Supra discharge 47019 (a). When the density is higher (b), there is no sign of supra thermal electrons.

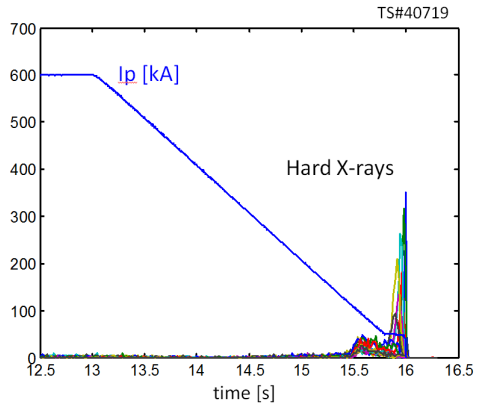

Figure 13: HXR data from the vertical camera (channels 1-21) in the energy range $E_{HXR} = 20 - 200$ keV. The HXR emission produced in the current ramp down in 40719 is a signature of suprathermal electrons, whereas in the higher density discharge 40721 no HXR emission is detected.

mentum, the full 2-D guiding-center momentum dynamics is taken into account, numerically manageable through a bounce-averaged description. The effect of magnetic trapping of the electrons in a non-uniform magnetic field configuration, known as the magnetic mirror effect, has been investigated, revealing reduction of both Dreicer and avalanche mechanisms off the magnetic axis. An analytical expression for avalanche growth rate accounting for magnetic trapping is derived. It is in agreement with numerical simulations and shows that a significant proportion of secondary electrons are knocked into the trapped region off the magnetic axis. The reduction of the off axis growth rate implies that the time scale of runaway formation is longer at the edge than close to the center, which means that potential loss mechanisms such as radial electron transport could compete with the acceleration of runaway electrons at the edge.

Moreover, quantifying the relative importance of avalanche generation as a function of plasma temperature and electric field strength, the simulations reveal that runaway electrons originating from knock-on collisions completely dominate at low temperature and electric field strength and likely play a significant role in runaway generation processes in several tokamaks with data from non-disruptive scenarios that are presented in Ref. [14]. The onset of runaway electrons found in these experiments are related to LUKE simulations of corresponding electric field and temperature in order to gauge the importance of the avalanche effect, revealing that knock-on collisions play a significant role also in non-disruptive scenarios. The LUKE calculations predict runaway electron generation also in a near critical field, in agreement with collisional theory if no other runaway electron loss mechanisms than collisional damping are present. However, the time to generate runaway electrons can be significantly large compared to the duration of the phase in which $E/E_c > 1$ in experiments. In

addition, the required time for runaway electron formation is very sensitive to the bulk electron temperature. The lack of runaway electron signatures near the critical electric field could therefore be explained by the long time scale required for their formation. To understand this discrepancy between observations and theory, the existence of additional loss mechanisms that dominate during the current flattop must be addressed. One possible candidate is transport of fast electrons due to magnetic field perturbations [20]. Once such additional runaway electron loss mechanisms have been identified, the LUKE code may form an excellent test bed for quantifying such effects, which will be the objective of future work.

Acknowledgement This work has been carried out within the framework of the EUROfusion Consortium and has received funding from the Euratom research and training programme 2014-2018 under grant agreement No 633053. The views and opinions expressed herein do not necessarily reflect those of the European Commission.

References

[1] T. C. Hender, J.C Wesley, J. Bialek, A. Bondeson, A.H. Boozer, R.J. Buttery, A. Garofalo, T.P Goodman, R.S. Granetz, Y. Gribov, O. Gruber, M. Gryaznevich, G. Giruzzi, S. Günter, N. Hayashi, P. Helander, C.C. Hegna, D.F. Howell, D.A. Humphreys, G.T.A. Huysmans, A.W. Hyatt, A. Isayama, S.C. Jardin, Y. Kawano, A. Kellman, C. Kessel, H.R. Koslowski, R.J. La Haye, E. Lazzaro, Y.Q. Liu, V. Lukash, J. Manickam, S. Medvedev, V. Mertens, S.V. Mirnov, Y. Nakamura, G. Navratil, M. Okabayashi, T. Ozeki, R. Paccagnella, G. Pautasso, F. Porcelli, V.D. Pustovitov, V. Riccardo, M. Sato, O. Sauter, M.J. Schaffer, M. Shimada, P. Sonato, E.J. Strait, M. Sugihara, M. Takechi, A.D. Turnbull, E. Westerhof, D.G. Whyte, R. Yoshino, H. Zohm, the ITPA MHD, Disruption, and Magnetic Control Topical Group. MHD stability, operational limits and disruptions. *Nucl. Fusion*, 47:S128–S202, 2007.

[2] J. Decker and Y. Peysson. DKE: A fast numerical solver for the 3D drift kinetic equation. Technical Report EUR-CEA-FC-1736, Euratom-CEA, 2004.

[3] M.N. Rosenbluth and S.V. Putvinski. Theory for avalanche of runaway electrons in tokamaks. *Nucl. Fusion*, 37(10):1355–1362, 1997.

[4] J.A. Wesson, R.D. Gill, M. Hugon, F.C. Schüller, J.A. Snipes, D.J. Ward, D.V. Bartlett, D.J. Campbell, P.A. Duperrex, A.W. Edwards, R.S. Granetz, N.A.O. Gottardi, T.C. Hender, E. Lazzaro, P.J. Lomas, and N. Lopes C. Disruptions in JET. *Nuclear Fusion*, 1989.

[5] M. Tavani, M. Marisaldi, C. Labanti, F. Fuschino, A. Argan, A. Trois, P. Giommi, S. Colafrancesco, C. Pittori, F. Palma, M. Trifoglio, F. Gianotti, A. Bulgarelli, and V Vittorini. Terrestrial gamma-ray flashes as powerful particle accelerators. *Phys. Rev. Lett.*, 2011.

[6] H. Dreicer. Electron and ion runaway in a fully ionized gas. i. *Phys. Rev.*, 115(2):238–249, 1959.

[7] J. W. Connor and R. J. Hastie. Relativistic limitations on runaway electrons. *Nucl. Fusion*, 15:415–424, 1975.

[8] M. Lehnen, A. Alonso, G. Arnoux, N. Baumgarten, S.A. Bozhenkov, S. Brezinsek, M. Brix, T. Eich, S.N. Gerasimov, A. Huber, S. Jachmich, U. Kruezi, P.D. Morgan, V.V. Plyusnin, C. Reux, V. Riccardo, G. Sergienko, M.F. Stamp, and JET EFDA contributors. Disruption mitigation by massive gas injection in JET. *Nuclear Fusion*, 51(12), 2011.

[9] M. Lehnen, S.S. Abdullaev, G. Arnoux, S.A. Bozhenkov, M.W. Jakubowski, R. Jaspers, V.V. Plyusnin, V. Riccardo, and U. Samm. Runaway generation during disruptions in JET and TEXTOR. *Journal of Nuclear Materials*, 390-391, 2009.

[10] E. M. Hollmann, P. B. Aleynikov, T. Fülöp, D. A. Humphreys, V. A. Izzo, M. Lehnen, V. E. Lukash, G. Papp, G. Pautasso, F. Saint-Laurent, and J. A. Snipes. Status of research toward the iter disruption mitigation system. *Physics of Plasmas*, 22:021802, 2015.

[11] E.M. Hollmann, P.B. Parks, D.A. Humphreys, N.H. Brooks, N. Commaux, N. Eidietis, T.E. Evans, R. Isler, A.N. James, T.C. Jernigan, J. Munoz, E.J. Strait, C. Tsui, J. Wesley, and J.H. Yu. Effect of applied toroidal electric field on the growth/decay of plateau-phase runaway electron currents in diii-d. *Nuclear Fusion*, 51, 2011.

[12] A. Bondeson. MHD modelling of density limit disruptions in tokamak. *Nucl. Fusion*, 31:1695–1716, 1991.

[13] A.V. Nedospasov. Thermal quench in tokamaks. *Nucl. Fusion*, 48, 2008.

[14] R. S. Granetz, B. Esposito, J. H. Kim, R. Koslowski, M. Lehnen, J. R. Martin-Solis, C. Paz-Soldan, T. Rhee, J. C. Wesley, and L. Zeng. An ITPA joint experiment to study runaway electron generation and suppression. *Physics of Plasmas*, 2014.

[15] G.T.A. Huysmans and O. Czarny. MHD stability in X-point geometry: simulation of ELMs. *Nuclear Fusion*, 47, 2007.

[16] C. Moller. *Annalen der Physik (Leipzig)*, 14:531–585, 1932.

[17] S. C. Chiu, M.N. Rosenbluth, R.W. Harvey, and V.S. Chan. Fokker-planck simulations of knowk-on electron runaway avalanche and bursts in tokamaks. *Nucl. Fusion*, 38(11):1711–1721, 1998.

[18] R.M. Kulsrud, Y.-C. Sun, N.K. Winsor, and H.A. Fallon. Runaway electrons in a plasma. *Phys. Rev. Lett.*, 31(11):690–693, 1973.

[19] L. G. Eriksson and P. Helander. Simulation of runaway electrons during tokamak disruptions. *Comp. Phys. Comm.*, 154:175–196, 2003.

[20] L. Zeng, H. R. Koslowski, Y. Liang, A. Lvovskiy, M. Lehnen, D. Nicolaiand J. Pearson, M. Rack, H. Jaegers, K. H. Finken, K. Wongrachand Y. Xu, and the TEXTOR team. Experimental observation of a magnetic-turbulence threshold for runaway-electron generation in the TEXTOR tokamak. *Phys. Rev. Letters*, 110:235003, 2013.

[21] S. Ejima, R.W. Callis, J.L. Luxon, R.D. Stambaugh, T.S. Taylor, and J.C. Wesley. Volt-second analysis and consumption in Doublet III plasmas. *Nuclear Fusion*, 22(10), 1982.

[22] T. WIJNANDS and G. MARTIN. An advanced plasma control system for Tore Supra. *FUSION TECHNOLOGY*, 32:471–486, 1997.

[23] M. Vlainic et al. Analyzing the first achieved runaway electron plateau in COMPASS tokamak. *To be submitted to Journal of Plasma Physics*, 2015.

A Appendix

Derivation of toroidicity dependent avalanche growth rate

As described in Sec. 3, the avalanche growth rate is evaluated by the flux surface averaged knock-on source term in Eq. 10 where the lower integration boundary is set by the maximum of the critical momentum p_c and the momentum defining the boundary of a passing and a trapped electron p_T, given by the trapping condition in Eq. 29. For finite E/E_c, the critical momentum $p_c > 0$. As the growth rate is averaged over the poloidal angle, $p_{min} \to p_c$ as the high field side is approached ($p_T \to 0$ as $\theta \to \pi$). The growth rate becomes:

$$\frac{dn_r}{dt_n}(\theta,\epsilon) = \frac{1}{2}\frac{1}{\ln\Lambda^\dagger}\bar{n}_e\bar{n}_r\frac{1}{\sqrt{1+p_{min}^2}-1} = \tag{33}$$

$$= \frac{1}{2}\frac{1}{\ln\Lambda^\dagger}\bar{n}_e\bar{n}_r \,\mathsf{min}\left(\frac{E}{E_c}, \frac{(1-\epsilon)^2}{2\epsilon(1+cos\theta)}\right). \tag{34}$$

The poloidal angle θ_{bound} where $p_c = p_T$ constitutes the boundary between the region where the avalanche rate is limited either by the drag force or by the magnetic trapping effect. This angle is obtained from the condition $p_c = p_T$:

$$1 + cos\theta_{bound} = (1-\epsilon)^2/(2\epsilon\frac{E}{E_c}) \to$$

$$\theta_{bound} = \pm\arccos((1-\epsilon)^2/(2\epsilon\frac{E}{E_c}) - 1).$$

If $\epsilon E/(E_c(1-\epsilon)^2) < 1/4$, p_c is the lower integration limit p_{min} and if $\epsilon E/(E_c(1-\epsilon)^2) > 1/4$, $p_{min} = p_T(\theta)$. Averaged over the flux surface according to volumic flux surface average the growth rate is:

$$
\begin{aligned}
< \quad & \frac{dn_r}{dt_n} >_V (\epsilon) = \qquad (35)\\
& = \frac{1}{\hat{q}} \left(\frac{1}{\pi} \int_0^{\theta_{bound}} \epsilon \frac{B_0(\epsilon)}{B_P} \frac{dn_r}{dt_n}(p_T(\theta)) d\theta + \frac{1}{\pi} \int_{\theta_{bound}}^{\pi} \epsilon \frac{B_0(\epsilon)}{B_P} \frac{dn_r}{dt_n}(p_c) d\theta \right) = \\
& = \frac{1}{2} \frac{1}{\ln \Lambda^\dagger} \bar{n}_e \bar{n}_r \times \\
& \times \left((1+\epsilon) \frac{B_p}{B} \frac{1}{\pi} \int_0^{\theta_{bound}} \frac{B_0(\epsilon)}{B_P} \frac{(1-\epsilon)^2}{2\epsilon(1+cos\theta)} d\theta + (1+\epsilon) \frac{E}{E_c} \frac{1}{\pi} \int_{\theta_{bound}}^{\pi} \frac{(1+\epsilon\cos(\theta))}{1+\epsilon} d\theta \right).
\end{aligned}
$$

In the above calculation circular concentric flux surfaces are considered so that $|\hat{\psi}\cdot\hat{r}|$=1, $r/R_p = \epsilon$ and

$$
\hat{q} = \int_0^{2\pi} \frac{d\theta}{2\pi} \epsilon \frac{B_0}{B_p} = \int_0^{2\pi} \frac{d\theta}{2\pi} \epsilon \frac{(1+\epsilon\cos(\theta))}{(1+\epsilon)} \frac{B}{B_p} = \frac{\epsilon}{(1+\epsilon)} \frac{B}{B_p}.
$$

The flux surface averaged growth rate takes the form:

$$
\begin{aligned}
< \quad & \frac{dn_r}{dt_n}(\theta,\epsilon) >_V = \frac{1}{2\ln\Lambda^\dagger} \bar{n}_e \bar{n}_r \frac{E}{E_c} \times \left(1 - \frac{\theta_{bound}}{\pi} - \frac{\epsilon}{\pi} \sin(\theta_{bound}) \right) \\
& + (1-\epsilon)^2 \frac{1}{2\epsilon\pi} \left((1-\epsilon) \tan(\theta_{bound}/2) + \epsilon\theta_{bound} \right) \qquad (36)\\
= \quad & \frac{1}{2\ln\Lambda^\dagger} \bar{n}_e \bar{n}_r \frac{E}{E_c} \times \\
& \times \left(1 - \frac{\theta_{bound}}{\pi} - \frac{\epsilon}{\pi} \sin(\theta_{bound}) + \frac{(1-\epsilon)^2 E_c}{2\epsilon\pi E} \left(\sqrt{1-\epsilon} \sqrt{4\epsilon E/E_c - (1-\epsilon)} + \epsilon\theta_{bound} \right) \right),
\end{aligned}
$$

where

$$
\tan(\theta_{bound}/2) = \frac{\sin(\theta_{bound})}{1 + cos(\theta_{bound})} = \frac{\sqrt{4\epsilon E/E_c - (1-\epsilon)}}{\sqrt{1-\epsilon}}.
$$

For $\epsilon E/E_c \gg 1$, $\theta_b \to \pi$ and the growth rate is reduced by a factor $(1-\epsilon)^2/\left(\pi\sqrt{\epsilon E/E_c}\right)$.